DE GRUYTER OPEN

ADVANCES IN MANUFACTURING SCIENCE AND TECHNOLOGY
Vol. 38, No. 3, 2014
DOI: 10.2478/amst-2014-0014

FRICTION MODELLING IN METAL CUTTING WITH INTEGRATED TOOL WEAR EFFECTS

Wit Grzesik, Krzysztof Żak

Summary

In this paper, friction in longitudinal turning operations when using chamfered uncoated ceramic tools is investigated. Both tool-chip and workpiece-tool interactions are integrated in the friction model. The values of three force components were consequently measured during tool wear tests at different cutting speeds they were used as input data for computing the friction and normal forces acting on the rake and flank faces and, as a result, for determining the relevant friction coefficients. It was observed that both friction coefficients are sensitive to tool wear progression depending on the cutting speed used. For comparison the values of friction coefficient were determined for orthogonal (2D) friction model. The 3D friction model was tested for the machining of spheroidal cast iron (SCI) using uncoated nitride ceramic inserts.

Keywords: friction, tool wear, metal cutting, silicon ceramic tool, spheroidal cast iron

Modelowanie tarcia w skrawaniu metali ze zintegrowanym wpływem zużycia narzędzia

Streszczenie

Prowadzono analizę tarcia w operacjach toczenia wzdłużnego z użyciem narzędzi z niepowlekanej ceramiki azotowej. W przyjętym modelu tarcia uwzględniono synergię oddziaływania na styku ostrze-wiór i przedmiot-ostrze. Wykonano pomiary wartości trzech sił składowych w czasie próby zużycia ostrza dla różnych wartości prędkości skrawania. Określane wartości użyto jako dane wejściowe do wyznaczenia wartości siły tarcia i siły normalnej, i w kolejności do wyznaczenia wartości określonego współczynnika tarcia. Stwierdzono, że współczynnik tarcia jest wrażliwy na przyrost zużycia narzędzia, zależnie od prędkości skrawania. W celu porównania wyznaczono wartości współczynnika tarcia dla ortogonalnego (2D) modelu tarcia. Weryfikację modelu 3D tarcia prowadzono dla skrawania żeliwa sferoidalnego z zastosowaniem niepowlekanych płytek ostrzowych z ceramiki azotowej.

Słowa kluczowe: tarcie, zużycie ostrza, skrawanie metal, narzędzia z ceramiki azotkowej, żeliwo sferoidalne

1. Introduction

Friction and tool wear are fundamental problems in machining research and modeling because they govern such process inputs as cutting forces, cutting energy, heat generation, and surface quality. The present knowledge of friction

Address: Prof. Wit GRZESIK, Krzysztof ŻAK, PhD Eng., Opole University of Technology, Faculty of Mechanical Engineering, 45-271 Opole, 5 Mikołajczyka Str., e-mail: w.grzesik@po.opole.pl, k.zak@po.opole.pl

in metal cutting seems to be insufficient to accurately model mechanical, thermal and tribological phenomena. Nowadays, the determination of the friction coefficient is generally based on the 2D orthogonal cutting model and Coulomb's law [1, 2]. In addition, other models based on adhesive interactions between the tool and the workpiece [3, 4] or a strain-hardening behaviour of the contact are proposed [5]. It is important that FEM-based cutting simulations using an inappropriate friction coefficient can generate more than 50% differences in cutting forces and the tool-chip contact length [6, 7]. On the other hand, the real cutting process is 3D in nature and consequently needs oblique cutting using cutting tools with defined inclination angle λ_s to be considered [1]. Typical values of inclination angle for commercial turning tools are small in the range of $\lambda_s = -6°$ to $-7°$ but for milling cutters, helical drills, broaching and shaving tools it is often in the order of tens of degrees. The problem becomes complex when using ceramic and CBN cutting inserts with negative rake angles for the chamfer in the range of $-20°$ to $-30°$, so as to protect cutting edges against premature failure [8, 9]. The problem is that the inclination and rake angles are the factors which change the components of the resultant cutting force. The third important factor is the sliding velocity which changes normal and shear loads [3, 10]. As a result, the friction which is defined as the relationship between normal force and friction force on the active parts of the cutting tool is changed as well [11, 12]. Previous studies on wear-modified friction [13, 14] indicated that for machining of spheroidal cast iron (SCI) with CBN tools, friction changes correspond to tool wear evolution Moreover, it was revealed in these studies that distinctly higher passive and feed forces occur in longitudinal turning with worn CBN tools. This paper proposes an integrated friction model for non-orthogonal cutting with chamfered fresh and worn Si_3N_4 ceramic tools.

2. Mechanistic modelling of friction in 3D cutting

2.1. Transformation of cutting forces

The forces acting on the rake and flank faces of the insert tip are presented in Fig. 1. Firstly, as shown in Fig. 1a, the resultant force F in the *xyz* coordinate system is resolved into three components- cutting F_z, feed F_x and passive (thrust) F_y forces. Secondly, the *lmn* coordinate system in which the *l* axis is parallel to and *m-n* plane is perpendicular to the cutting edge is introduced, so F_l, F_m and F_n components characteristic for oblique cutting are specified. According to the geometrical summation of forces in the Cartesian system:

$$\bar{F} = \bar{F}_x + \bar{F}_y + \bar{F}_z = \bar{F}_l + \bar{F}_m + \bar{F}_n \tag{1}$$

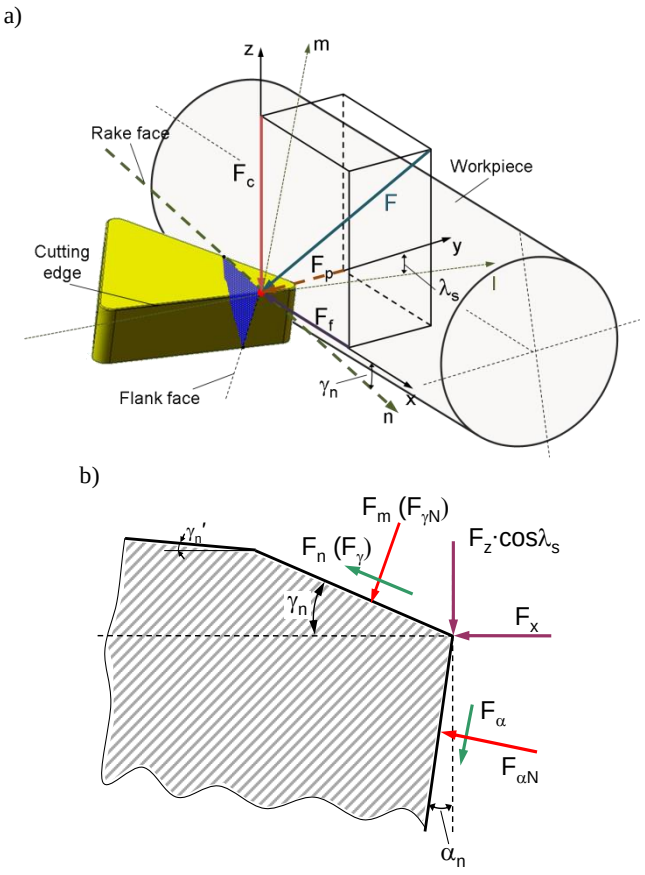

Fig. 1. Definition of coordinate systems (a) and forces acting on the cutting wedge (b)

As shown in Fig. 1a, the *lmn* system is obtained by rotating the *xyz* system by the λ_s angle around the *x* axis firstly and secondly around the *y* axis by the normal rake angle γ_n.

Hence, the transformation of force components from the *xyz* coordinate system to the *lmn* system using two unit rotating matrixes $[TM]_x$ and $[TM]_y$ [13] is given by Eqn. (2).

$$\begin{bmatrix} F_n \\ F_l \\ F_m \end{bmatrix} = [TM]_x [TM]_y \begin{bmatrix} F_x \\ F_y \\ F_z \end{bmatrix} = \begin{bmatrix} \cos\gamma_n & 0 & -\sin\gamma_n \\ -\sin\lambda_s \sin\gamma_n & \cos\lambda_s & -\sin\lambda_s \cos\gamma_n \\ \cos\lambda_s \sin\gamma_o & \sin\lambda_s & \cos\lambda_s \cos\gamma_n \end{bmatrix} \begin{bmatrix} F_x \\ F_y \\ F_z \end{bmatrix} \tag{2}$$

By solving matrix Eqn. (2) one obtains three equations which determine components F_l, F_m and F_n in terms of the measured F_x, F_y and F_z forces, as follows:

$$F_l = -F_x \sin\lambda_s \sin\gamma_n + F_y \cos\lambda_s - F_z \sin\lambda_s \cos\gamma_n \tag{3.1}$$

$$F_m = F_x \cos\lambda_s \sin\gamma_n + F_y \sin\lambda_s + F_z \cos\lambda_s \cos\gamma_n \tag{3.2}$$

$$F_n = F_x \cos\gamma_n - F_z \sin\gamma_n \tag{3.3}$$

It can be seen in Fig. 1b that the friction force on the rake face F_γ^{ob} is equal to F_n and the normal force $F_{\gamma N}^{ob}$ is equal to F_m. On the other hand, the friction and normal forces acting on the flank face are equal to

$$F_\alpha = F_z \cos\alpha_n - F_x \sin\alpha_n \tag{4.1}$$

$$F_{\alpha N} = -F_z \sin\alpha_n + F_x \cos\alpha_n \tag{4.2}$$

In the next step the friction and normal forces were utilized to calculating the friction coefficients related to the rake and flank faces.

2.2. Determination of friction models

When the friction force on the rake face (F_n) and the normal force (F_m) are determined using a set of Eqns. (3.1)-(3.3), and forces F_α and $F_{\alpha N}$ acting on the flank face are calculated by means of Eqns. (4.1) and (4.2), the average friction coefficients for the non-orthogonal (oblique) cutting related to the rake and flank faces are as follows:

$$\mu_{\gamma_{ob}} = \frac{F_\gamma^{ob}}{F_{\gamma N}^{ob}} = \frac{F_n}{F_m} \tag{5.1}$$

$$\mu_{\alpha_{ob}} = \frac{F_\alpha}{F_{\alpha N}} \tag{5.2}$$

On the other hand, the friction coefficient for orthogonal cutting is equal to [1]:

$$\mu_o = \mathrm{tg}\left[\mathrm{tg}^{-1}\left(\frac{F_z}{F_x} \right) + \gamma_o \right] \tag{6}$$

3. Experimental Procedure

3.1. Characteristics of machining process

Turning trials and wear tests were performed on the bars made of spheroidal cast iron, EN-GJS-500-7 grade [15], using a CNC turning center. Uncoated Si_3N_4 ceramic cutting inserts, CC6090 grade (Sandvik Coromant), denoted by symbol TNGA 16 04 08T02520 GC1690 which were clamped in PTNGR 2020 –16 tool holder were selected. The optical image of the insert corner with characteristic chamfer dimensions is presented in Fig. 2.

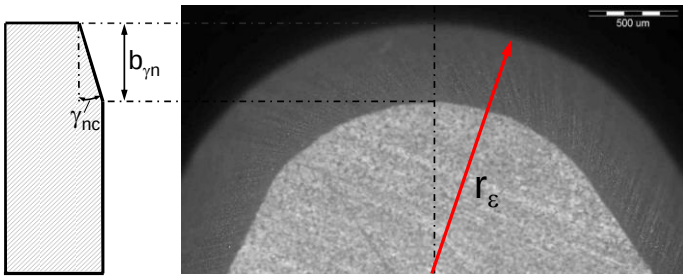

Fig. 2. Geometry of the cutting tool insert used – r_ε = 0.8 mm, $b_{\gamma n}$ = 0.20 mm, γ_{nc} = 20°

Nominal effective rake angle was equal to γ_{oe} = –6°, the chamfer angle was equal to γ_{nc} = –20° (the effective rake angle at the chamfer was γ_{nce} = –26°) and the tool cutting edge angle κ_r = 90°. The chamfer width was equal to 0.2 mm as shown in the wedge cross-section in Fig. 2. The following cutting parameters were selected: constant depth of cut a_p = 0.8 mm and a feed rate of 0.08 mm/rev and 0.12 mm/rev, and a variable cutting speed of 100, 160, 240, 320, 400 and 480 m/min. Relatively small values of feed rate in conjunction with a large chamfer width of 0.2 mm guarantee that the chip-rake contact is concentrated on the area of chamfer. In consequence, this fact allows relating all calculations of forces acting on the rake face to the chamfer angle (in Eqns. (3.1)-(3.3) $\gamma_n = \gamma_{nce}$).

3.2 Measurements and visualization techniques

Three components F_z, F_y and F_x of the resultant cutting force (Fig. 1a) were measured using a measurement system equipped with a Kistler 9257A piezoelectric dynamometer and a Kistler 5070 signal amplifier. The measured

data were recorded using a DasyLab v9.0 data acquisition program. Measurements of the wear scars on the flank face and visualizations of worn tips were carried out on a Leica optical microscope equipped with a CCD camera. Image processing was performed by means of an IM1000 program. Examinations of worn corners were carried out using a Hitachi S-3400N SEM microscope.

4. Experimental results and discussion

4.1. Measurements of tool wear

In this study the nose wear VB_C was measured in the *post-process* mode keeping the time intervals between several to dozens of seconds. An exemplary SEM image of the worn Si_3N_4 tip is presented in Fig. 3. Based on VB_C data recorded the wear curves were drawn as shown in Fig. 4. The critical value of nose wear VB_C was assumed to be about 0.3 mm.

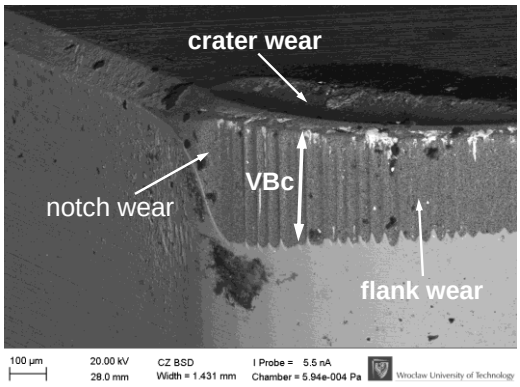

Fig. 3. Exemplary SEM image of tool wear in the corner area

For instance, Fig. 3 shows the configuration of worn TiN/Si_3N_4 tip after cutting test performed with the cutting speed of 400 m/min. In this case, the worn zone was visualized using SEM technique. As shown in Fig. 3 the crater wear is developed on the chamfered rake face which, in turn, changes tribological conditions in comparison to the initial ones. Fig. 4 shows the progress of the flank wear in the corner zone "C" depending on the cutting speeds applied. Evidently, the time required to achieve the critical value of VB_C wear indicator is a function of cutting speed. In general, the tool life is rather short and for instance for the medium cutting speed of 240 m/min it is about 2 min (the cutting length is about 480 m).

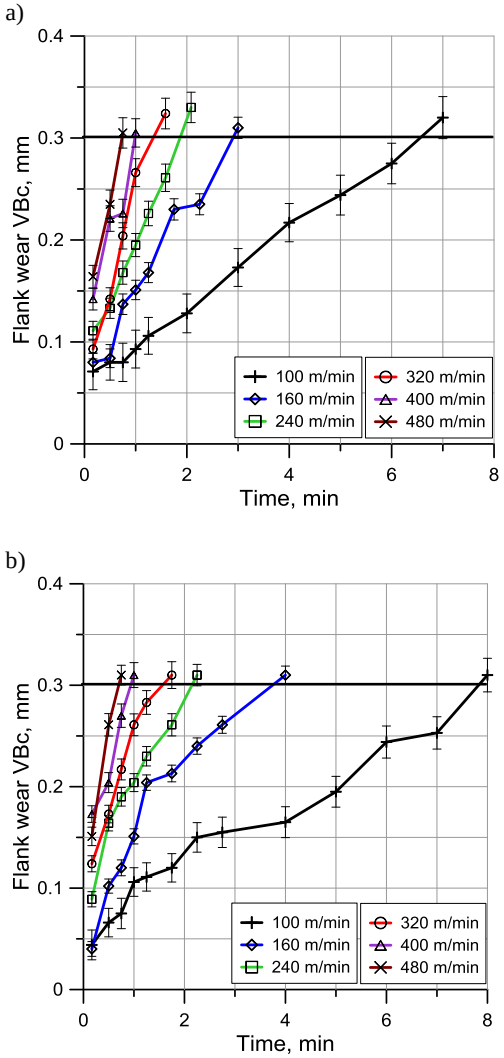

Fig. 4. Changes of tool flank wear VBc vs. time for different cutting speeds and a feed rate of: a) 0.08 mm/rev, b) 0.12 mm/rev

4.2. Measurements of forces during wear tests

This study includes extended measurements of forces as a basic source of the assessment of process instabilities during tool wear. The direct measurements include three components F_z, F_y and F_x of the resultant cutting force as shown in Fig. 5. In this case the forces were measured after the first 10 s of cutting which roughly corresponds to the running-in period. It can be seen in Fig. 5 that the value of the initial tool wear depends on the cutting speed used.

The first important effect which can be observed in Fig. 5 is that the radial force *Fy* increases when the cutting speed and integrally tool wear increases. Based on the measured values of F_z, F_y and F_x forces, the F_l, F_m and F_n components were computed using a set of Eqn. 3.1-3.3. In order to illustrate the absolute changes of the three componential forces F_z, F_x and F_y, their increments were determined as the differences between force values measured at the beginning (fresh tools) and the end (critically worn) of wear tests.

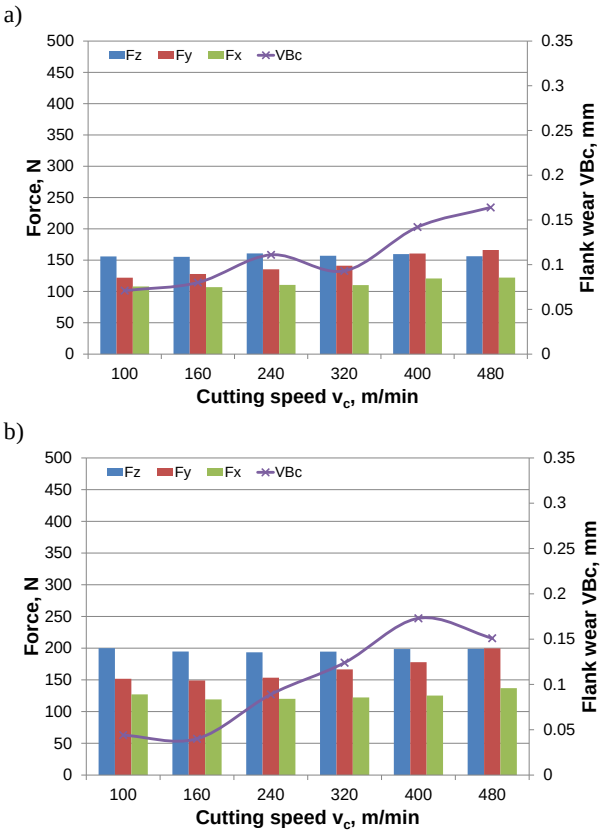

Fig. 5. Values of cutting forces and tool wear progress after 10 s cutting time: a) for feed rate f = 0.08 mm/rev, b) for feed rate f = 0.12 mm/rev

The comparison of the increments of F_z, F_y and F_x forces during tool wear shown in Figs. 6 and 7 reveals that they change in a specific manner depending on the feed value. For the lower feed rate of 0.08 mm/rev tool wear causes that the increments of the feed force F_x are the highest ones starting from the cutting speed of 160 m/min. In contrast, the increments of the cutting force *Fz* are the lowest ones, which additionally decrease when the cutting speed increases up to

480 m/min. According to Fig. 7, showing the increments of the force components *Fz*, *Fy* and *Fx* for the higher feed rate of 0.12 mm/rev, the most important is the increment of the passive (radial) force, which visibly overcame the increments of the feed force *Fx* documented previously in Fig. 6. It should be noted that in both these both cases the value of VBc indicator was roughly kept between 0.25 and 0.3 mm. This fact evidently confirms that the wear process causes that the cutting performed with the chamfered Si_3N_4 ceramic and CBN tools can be considered to be the oblique cutting [13]. The maximum increase of the F_x force determined for the cutting speed of 400 m/min is approximately of 500%. This fact can be explained in terms of intensive notch wear developing in the vicinity of the secondary cutting edge (exemplarily see SEM image in Fig. 3).

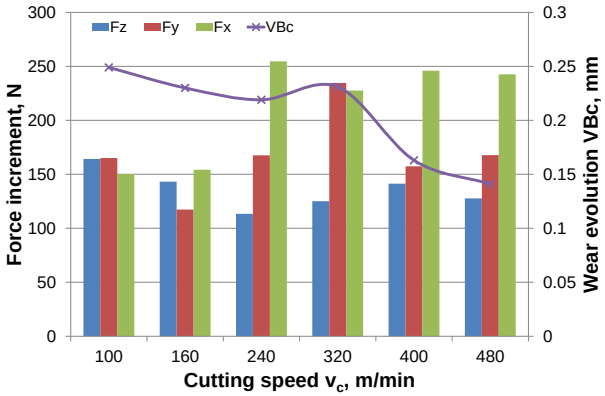

Fig. 6. Comparison of increments of cutting forces for worn tools and different cutting speeds keeping feed rate of 0.08 mm/rev

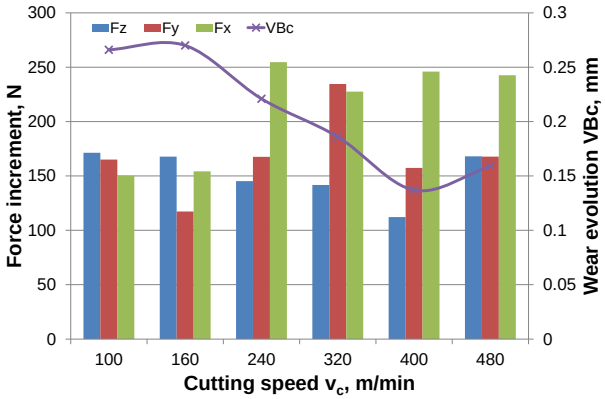

Fig. 7. Comparison of increments of cutting forces for worn tools and different cutting speeds keeping feed rate of 0.12 mm/rev

4.3. Determination of friction on the rake and flank faces during tool wear

It is obviously known in the tribology of the metal cutting process that the friction coefficient can exceed 1 distinctly especially at the flank face of uncoated HSS and carbide cutting tools. For instance, it is reported that due to severe adhesion between the flank/rake face and the fresh surface of the workpiece/chip the value of μ_α is 1-1.4 [16, 17]. Moreover, the contact conditions at this part of the wedge have elastic character without the seizure effect occurring at the rake face part adjacent to the cutting edge (Fig. 8a). This tribological evidence is confirmed by photo-elastic method in Fig. 8b. It is revealed that the shear stress τ_α on the flank face is visibly higher that the normal stress σ_α (Fig. 8b). The cutting temperature of 400°-500°C characteristic for machining SCI with ceramic tools is sufficient for the occurrence of severe adhesion at the flank face [18, 19]. This fact corresponds well to the changes of the friction coefficient at the flank face presented in Fig. 9 and 10.

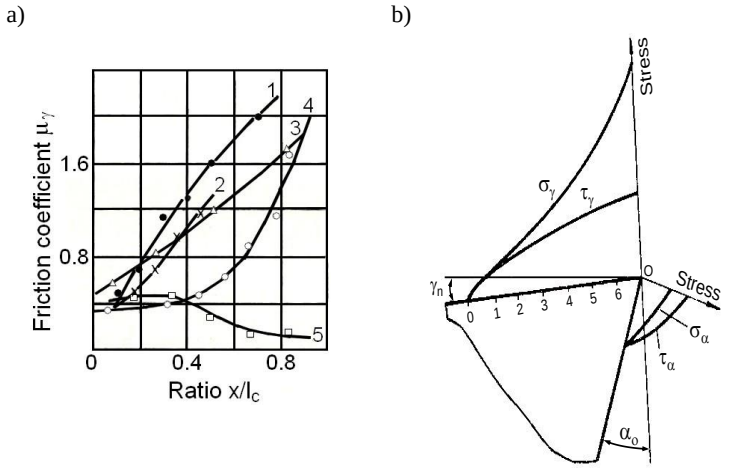

Fig. 8. Distribution of friction coefficient on the rake face (a) by Poletika and Uteshev (1), Andreev (2), Kattwinkel (3), Takeyama and Usui (4), Chandrasekaran and Kapoor (5) [10] and contact stresses on the rake and flank faces (b) [20]

Figures 9 and 10 present the relevant changes of the friction coefficients $\mu_{\gamma ob}$ and μ_α obtained at the beginning and the end of the wear tests of Si_3N_4 tips for a range of cutting speeds and two feed rates of 0.08 and 0.12 mm/rev respectively. They were determined by means of Eq. 5.1 using force values specified in Fig. 5-7. For comparison, relevant changes of friction coefficient μ_o are computed for the simple orthogonal model using Eqn. 6.

It is clear from the plots $\mu_{\gamma ob}$ and $\mu_{\gamma o}$ *vs.* cutting speed presented in Fig. 9 and 10 that the coefficient of friction on the rake face is more sensitive to the cutting speed variations than the friction coefficient on the flank face. However, differences between values of friction coefficient obtained for fresh (unworn) (Fig. 9) and worn (Fig. 10) cutting edges can be related to different normal loads determined by two mechanical models considered. This is because the increments of the radial force *Fy* are the highest ones at the end of wear tests, as shown in Figs. 6 and 7.

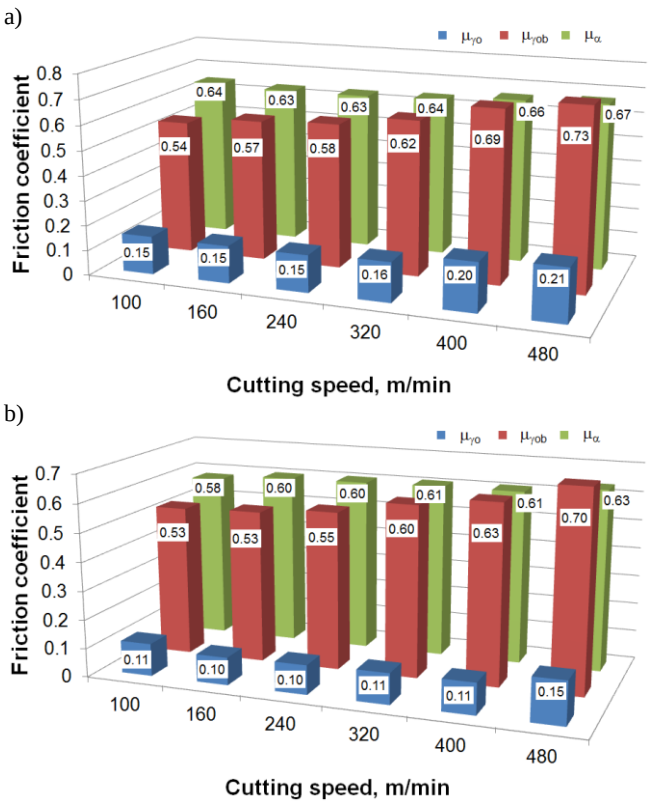

Fig. 9. Comparison of μ values obtained for orthogonal and oblique cutting models for fresh cutting insert: a) f = 0.08 mm/rev, b) f = 0.12 mm/rev

Similar variations of the coefficient of friction for ceramic materials are documented in Refs. [21] and [22] respectively. In particular, the tendency of μ to decrease with the wear progress can be related to the thermal effect occurring visibly at the temperature above 400-500°C [15, 22]. In the machining of spheroidal cast iron with the cutting speed of 240-480 m/min, the measured

maximum interface temperature ranges from about 450°C to 520°C and this effect is highly feasible [22].

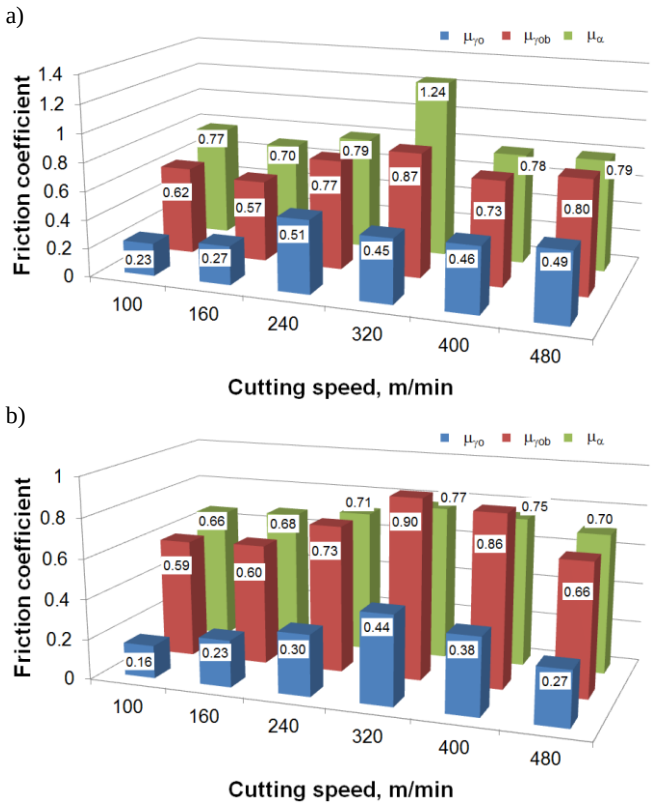

Fig. 10. Comparison of μ values obtained for orthogonal and oblique cutting models for worn cutting insert: a) f = 0.08 mm/rev, b) f = 0.12 mm/rev

As suggested in section 4.3, friction at the flank face is predominantly controlled by the adhesion between the tool and a chemically clean machined surface. The differences in the values of μ_α (determined by means of Eqn. 5.2) caused by an increased adhesion intensity is clearly illustrated for the cutting speed of 320 m/min in Fig. 10a. With the increase of cutting speed the contact temperature increases which activates adhesion between the silicon nitride ceramic and SCI workpiece [23]. As a result, at the cutting speeds 320-480 m/min the values of μ_α approach 0.9 (see Fig. 10b).

The comparison of the values of coefficients of friction on the rake face $\mu_{\gamma o}$, $\mu_{\gamma ob}$ and μ_α determined for fresh tools for a variable cutting speed and two selected feed rates is shown in Fig. 9. It is evident in Fig. 9 that the values of friction coefficients $\mu_{\gamma o}$ and $\mu_{\gamma ob}$ differ distinctly from each other. In majority of

cutting tests, values of $\mu_{\gamma ob}$ are of about five times higher than friction coefficients computed for the classical orthogonal model represented by Eqn. 6.

It should be noted in Fig. 9 that at the beginning of wear tests, i.e. for practically fresh Si_3N_4 uncoated ceramic inserts the differences between values of $\mu_{\gamma o}$ practically do not depend on the cutting speed used. On the other hand, the variations of $\mu_{\gamma ob}$ are relatively small at all cutting speeds. It is interesting to note that for fresh tools the values of friction coefficients determined for rake and flank faces are comparable (difference in same cases are about 0.1).

As shown in Fig. 10b, the wear of a Si_3N_4 ceramic insert causes the friction coefficient to increase in comparison to the result obtained for fresh tools, and this effect is more pronounced for orthogonal-based $\mu_{\gamma o}$ which does not consider changes of all three componential forces integrally. It can be noted that the values of $\mu_{\gamma o}$ approach 0.5 for the higher cutting speed. It is interesting to note that for uncoated ceramic inserts similar behaviour of μ_{α} in comparison to $\mu_{\gamma ob}$ resulting from the wear progress is observed. This fact is in sharp contrast to coated ceramic inserts for which at the end of the wear test performed with high cutting speeds the values of μ_{α} are about 2 [24]. This fact evidently indicates different tribological behaviour of the rake and flank faces during the tool wear for uncoated and coated Si_3N_4 cutting tools.

5. Conclusions

The following original results were produced from this study:

- A new 3D model of friction for non-orthogonal cutting, incorporating tool wear is developed and compared with the 2D orthogonal model-based friction.
- Substantial differences between the values of friction coefficient determined for orthogonal and non-orthogonal cutting were revealed.
- The values of friction coefficient determined for worn tools are higher than those obtained for slightly worn tools (due to very rapid running-in process). They are about 0.5-0.7 and 0.6-0.9 respectively.
- The values of friction coefficient for the rake and flank faces are comparable for fresh and worn tools.
- The proposed methodology can be applied to determining the values of friction coefficient for a selected time during the wear test.

References

[1] W. GRZESIK: Advanced machining processes of metallic materials. Elsevier, Amsterdam 2008.
[2] M.C. SHAW: Metal cutting principles. Clarendon Press, Oxford 1989.

[3] F. ZEMZENI, J. RECH, W. Ben SALEM, Ph. KAPSA: Identification of friction and heat partition model at tool-chip-workpiece interfaces in dry cutting of an INCONEL 718 alloy with CBN and coated carbide tools. *Advances in Manufacturing Science and Technology*, **38**(2014)1, 5-21.
[4] W. GRZESIK: Experimental investigation of the influence of adhesion on the frictional conditions in the cutting process. *Tribology International*, **32**(1999), 15-23.
[5] T.H.C. CHILDS: Friction modeling in metal cutting. Wear, **260**(2006), 310-318.
[6] T. ÖZEL: The influence of friction models on finite element simulations of machining. *Int. Journal of Machine Tools and Manufacture***, 46**(2006), 518-530.
[7] P.J. ARRAZOLA, D. UGARTE, X. DOMINGUEZ: A new approach for the friction identification during machining through the use of finite element modeling. *Int. Journal of Machine Tools and Manufacture***. 48**(2008), 173-183.
[8] H. REN, Y. ALTINTAS: Mechanics of machining with chamfered tools. *Trans. of ASME. Journal of Manufacturing Science and Engineering*, **122**(2000), 650-659.
[9] J.M. ZHOU, H. WALTER, M. ANDERSSON, J.E. STAHL: Effect of chamfer angle on wear of PCBN cutting tool. *Int. Journal of Machine Tools and Manufacture*, **43**(2003), 301-305.
[10] M.F. POLETIKA: Contact Loads on the Active Parts of Cutting Tools (in Russian). Mašinostroenie, Moscov 1969.
[11] W. GRZESIK: The mechanics of continuous chip formation in oblique cutting with single-edged tool – Part I. Theory. *Int. Journal of Machine Tools and Manufacture*, **30**(1990), 359-371.
[12] W. GRZESIK: The mechanics of continuous chip formation in oblique cutting with single-edged tool – Part II. Experimental verification of the theory. *Int. Journal of Machine Tools and Manufacture*, **30**(1990), 373-388.
[13] W. GRZESIK, K. ŻAK: Friction quantification in the oblique cutting with CBN chamfered tools. *Wear*, **304**(2013), 36-42.
[14] W. GRZESIK, D. KOWALCZYK, K. ŻAK: A new mechanistic friction model for the oblique cutting with tool wear effect. *Tribology International*, **66**(2013), 49-53.
[15] W. GRZESIK, P. KISZKA, D. KOWALCZYK, J. RECH, Ch. CLAUDIN: Machining of nodular cast iron (PF-NCI) using CBN tools. Proc. 4th HPC Conf., Zurich, *Procedia CIRP*, (2012)1**,** 500-504.
[16] I.M. Hutchings: Tribology. Friction and Wear of Engineering Materials. Edward Arnold, London 1992.
[17] W. GRZESIK: The influence of thin hard coatings on frictional behaviour in the orthogonal cutting process. *Tribology International*, **33**(2000), 131-140.
[18] W. GRZESIK, K. ŻAK: Mechanical, thermal and tribological aspect of the machining process of nodular iron with coated carbide and ceramic tools. *Advances in Manufacturing Science and Technology*, **33**(2009)1, 31-43.
[19] W. GRZESIK, J. MAŁECKA, D. KOWALCZYK, P. KISZKA: Wear behaviour of nitride ceramic cutting tools in the machining of nodular cast iron. *Advances in Manufacturing Science and Technology*, **35**(2011)2, 5-16.
[20] K. HOLMBERG, A. MATTHEWS: Coating Tribology. Elsevier, Amsterdam 1998.
[21] V.A. OSTAFEV: Physical fundamentals of the metal cutting process (in Russian). Visša Škola, Kiev 1976.

[22] W. GRZESIK: An investigation of the thermal effects in orthogonal cutting associated with multilayer coatings. *CIRP Annals Manufacturing Technology*, **50**(2001), 53-55.
[23] W. GRZESIK, J. MAŁECKA: Documentation of tool wear progress in the machining of nodular ductile iron with silicon nitride-based tools. *CIRP Annals Manufacturing Technology*, **60**(2011), 121-124.
[24] W. GRZESIK, J. RECH, K. ŻAK: Determination of friction in metal cutting with tool wear and flank face effects. *Wear*, **317**(2014), 8-16.

Received in July 2014